Aqp5 $^{-/-}$ mice exhibit reduced maximal body O_2 consumption under cold exposure, normal pulmonary gas exchange, and impaired formation of brown adipose tissue

Samer Al-Samir[1], Ali Önder Yildirim[2], Venkataramana K Sidhaye[3], Landon S King[3], Gerhard Breves[4], Thomas M. Conlon[2], Claudia Stoeger[5], Valerie Gailus-Durner[5], Helmut Fuchs[5], Martin Hrabé de Angelis[5,6,7], Gerolf Gros[1]*, Volker Endeward[1]

1 Zentrum Physiologie, AG Vegetative Physiologie – 4220 –, Medizinische Hochschule Hannover, Germany

2 Comprehensive Pneumology Center (CPC), Institute of Lung Biology and Disease, Helmholtz Zentrum München, 85764 Munich, Germany, Member of the German Center for Lung Research (DZL).

3 Department of Medicine, Div. Pulmonary and Critical Care Medicine, Johns Hopkins School of Medicine, Baltimore, Maryland, USA

4 Institut für Physiologie und Zellbiologie, Tierärztliche Hochschule Hannover, 30173 Hannover, Germany

5 Institute of Experimental Genetics, German Mouse Clinic, Helmholtz Zentrum München, German Research Center for Environmental Health (GmbH), 85764 Neuherberg, Germany

6 German Center for Diabetes Research (DZD), 85764 Neuherberg, Germany

7 Chair of Experimental Genetics, TUM School of Life Sciences, Technische Universität München, 85354 Freising, Germany

Running Head: Aquaporin 5 and brown adipose tissue

Corresponding authors: *

Dr. Gerolf Gros
Zentrum Physiologie
AG Vegetative Physiologie 4220
Medizinische Hochschule Hannover
30625 Hannover / Germany
Tel. +49 511 532 2735
Fax: +49 511 532 2938
e-mail: Gros.Gerolf@MH-Hannover.de

Dr. Samer Al-Samir
Zentrum Physiologie
AG Vegetative Physiologie 4220
Medizinische Hochschule Hannover
30625 Hannover / Germany
e-mail: Al-Samir.Samer@MH-Hannover.de

Dr. Volker Endeward
Zentrum Physiologie
AG Vegetative Physiologie
Medizinische Hochschule Hannover
30625 Hannover /Germany
e-mail: Endeward.Volker@MH-Hannover.de

Supplemental Data:

https://figshare.com/articles/figure/AQP5_KO_Mice_Lung_Parameters/20097401

DOI: https://doi.org/10.6084/m9.figshare.20097401.v2

Abstract

The fundamental body functions that determine maximal O_2 uptake ($\dot{V}_{O2,max}$) have not been studied in Aqp5 $^{-/-}$ (aquaporin 5, AQP5) mice. We measured $\dot{V}_{O2,max}$ to globally assess these functions and then investigated why it was found altered in Aqp5 $^{-/-}$ mice. $\dot{V}_{O2,max}$ was measured by the Helox technique, which elicits maximal metabolic rate by intense cold exposure of the animals. We found $\dot{V}_{O2,max}$ reduced in Aqp5 $^{-/-}$ mice by 20 - 30% compared to WT. Since AQP5 has been implicated to act as a membrane channel for respiratory gases, we studied whether this is due to the known lack of AQP5 in the alveolar epithelial membranes of Aqp5 $^{-/-}$ mice. Lung function parameters as well as arterial O_2 saturation were normal and identical between Aqp5 $^{-/-}$ and WT mice, indicating that AQP5 does not contribute to pulmonary O_2 exchange. The cause for the decreased $\dot{V}_{O2,max}$ thus might be found in decreased O_2 consumption of an intensely O_2-consuming peripheral organ such as activated BAT. We found indeed that absence of AQP5 greatly reduces the amount of interscapular BAT formed in response to 4 weeks' cold exposure, from 63% in WT to 25% in Aqp5 $^{-/-}$ animals. We conclude that lack of AQP5 does not affect pulmonary O_2 exchange, but greatly inhibits transformation of white to brown adipose tissue. Since under cold exposure BAT is a major source of the animals' heat production, reduction of BAT likely causes the decrease in $\dot{V}_{O2,max}$ under this condition.

Key Words:

Aquaporin 5, oxygen transport across membranes, gas channels, alveolar-capillary barrier, pulmonary diffusion capacity, cold-induced brown adipose tissue, cold acclimatization of mice

Introduction

Maximal oxygen consumption of the body, $\dot{V}_{O2,max}$, is a quantity that critically depends on a large number of crucial vital parameters such as cardiac output, pulmonary gas exchange, O_2 and CO_2 transport in the blood, microcirculation,

skeletal muscle mass and its fiber characteristics. Thus, $\dot{V}_{O2,max}$ can be used to obtain a global assessment of many basic parameters of an organism. Previously, we have used this parameter to characterize aquaporin-1 (AQP1) and aquaporin-9 (AQP9) knockout mice. We have reported that AQP9-ko mice exhibit normal $\dot{V}_{O2,max}$, while AQP1-ko mice have a $\dot{V}_{O2,max}$ reduced by 16% (1). Arterial oxygen saturation as measured by pulse oximetry in the carotid artery was normal and identical in AQP1-ko and in WT mice. Thus, pulmonary gas exchange in AQP1 mice is not affected by the lack of AQP1. Searching for the cause of the reduction of $\dot{V}_{O2,max}$, we observed in a subsequent study – in partial agreement with an earlier study (2) – that the left ventricles of AQP1-ko mice possess a reduced muscle mass and wall thickness (3), which is expected to result in a diminished maximal cardiac output in $Aqp1^{-}/^{-}$ mice.

We note that it is the Helox technique that we have used in the aforementioned as well as in the present study to assess $\dot{V}_{O2,max}$. This technique measures oxygen consumption under exposure of the mice to 4°C with the animals respiring a gas mixture of He and O_2 that is cooled down also to 4°C. This results in a marked heat loss of the animals, mainly by their ventilation, which increases oxygen consumption to maximal levels in order to maintain body core temperature. $\dot{V}_{O2,max}$ obtained by the Helox method has repeatedly been shown to be – with exceptions - identical to that obtained by forced wheel or treadmill running (4–6).

In the present study, we apply the Helox technique to a comparison of $Aqp5^{-}/^{-}$ and WT mice. AQP5 is an aquaporin that conducts water like AQP1 and AQP9, but does not conduct glycerol as the aquaglyceroproteins do. Recently, it has been shown to conduct CO_2 in addition (7, 8), as has earlier been shown extensively for AQP1 (7, 9–12). Besides AQP1 and AQP5, several other aquaporins such as AQP0, AQP4, AQP6 and AQP9 have been demonstrated to act as channels for CO_2 besides for water (7, 11). The main pathway through aquaporins used by CO_2, the central pore of the aquaporin tetramer, has been shown in the case of AQP1 and AQP4 to also act as a channel for O_2 (9, 13–15). It has been pointed out that the relative role of protein gas channels will depend on the intrinsic gas permeability of the membrane considered (16). It has also been pointed out that the membrane protein content and membrane cholesterol affect this intrinsic permeability. In the case of O_2 permeability, it has been shown that membrane protein can reduce the apparent gas

permeability of the membrane by 30-40% (17). However, a much more potent effector of intrinsic membrane gas permeability seems to be cholesterol, which can decrease membrane CO_2 permeability by 2-3 orders of magnitude (18), and can raise intrinsic O_2 permeability by one order of magnitude (19). Thus, high membrane cholesterol can very effectively make protein CO_2 channels the dominant pathway for CO_2 across the membrane, and even in the case of O_2 permeation across high-cholesterol membranes the intrinsic membrane O_2 permeability is still so low that O_2 fluxes across the membrane might be noticeably enhanced by gas channels (19). Thus, in the present case of AQP5, it is conceivable that this protein could also play a role as a channel for O_2.

When searching for AQP5's function, a further aspect to be considered is its distribution in the organs of the body. According to several authors (20–22) a major localization of AQP5 is in the lung, with strong staining of the apical membranes of type I alveolar epithelium and also staining in the more proximal airways from bronchi up to the trachea. In addition, there are significant localizations in several smaller exocrine glands such as the submandibular gland, lacrimal gland, and to a weaker extent in the parotid and sublingual glands. Stronger staining has in addition been observed in the eye, and AQP5 expression has recently also been reported in brown adipose tissue (23). AQP5 appeared absent in heart, skeletal muscle, red blood cells as well as in the gastrointestinal tract (22). Thus, in contrast to $Aqp1^{-}/^{-}$ mice, cardiac function, as well as skeletal muscle function, should not be affected in $Aqp5^{-}/^{-}$ mice.

In this article, we aim to determine the function of AQP5 in oxygen transport in the body, next to its known role of fluid transport in glandular secretion in the above-mentioned glands. For this purpose, we first measure $\dot{V}_{O2,max}$ of $Aqp5^{-}/^{-}$ and WT mice. Since we find $\dot{V}_{O2,max}$ to be markedly reduced in $Aqp5^{-}/^{-}$ mice, we then investigate whether maximal body oxygen consumption is reduced a) due to a limitation on the side of O_2 uptake, i.e. in the lung, or b) by a limitation on the side of O_2 entry into a peripheral O_2-consuming organ. On the peripheral side, we study brown adipose tissue (BAT), because this tissue can exhibit an extremely high oxygen consumption, whereas two other potentially intense oxygen consumers, heart and skeletal muscle, do not express AQP5 und thus should not be affected in $Aqp5^{-}/^{-}$ animals.

Methods

Animals. – Breeding pairs of heterozygous aquaporin-5 KO mice bred on a C57Bl/6 background were those generated in Dr. Anil Menon's lab (24) and thoroughly characterized by the same group (24, 25). This mouse line, which was subsequently used in Dr. Venkatamarana K. Sidhaye's lab (26) and in the present work, was demonstrated to lack AQP5 protein in several localizations (several exocrine glands and lung) (24, 25). These mice were intercrossed with C57Bl/6 mice to obtain homozygous AQP5-KO and WT littermate controls, as ascertained by PCR genotyping. DNA was obtained from ear punchings used with the specific primers Aqp5-Int3F: ACCC CTTG ACAG CGTC TCCA, Aqp5-Int3R: GACA GGAT TCCC AATC CCAC , and Aqp5-RPGKO: GCAT GCTC CAGA CTGC CTTG G in one single PCR reaction. The mice used in this study had an age of between 75 and 90 days. All animal experiments were approved by the Niedersächsisches Landesamt für Verbraucherschutz und Lebensmittelsicherheit (No. 33.12-42502-04-16/2328). At the German Mouse Clinic (27, 28), mice were maintained in IVC cages with water and standard mouse chow according to the directive 2010/63/EU, German laws and GMC housing conditions (www.mouseclinic.de). All tests were approved by the Regierung von Oberbayern.

AQP5 Western Blots. – We have ascertained the absence of AQP5 in the KO animals of our present breed by performing Western Blots from lung tissue homogenate of KO and WT mice. To obtain the homogenates, animals were killed via cervical dislocation und the lungs removed. Connecting tissue and the trachea were removed from the isolated lung. Tissue was suspended in phosphate buffered saline with 0.25 M glucose, 1mM PMSF and 4 µg/ml leupeptin. The vessel containing the lung tissue was immersed in ice water and the tissue homogenized with an Ultra-Turrax Tissue homogenizer (IKA Werk, Staufen, Germany) by 4 short 3-second bursts. The homogenate was then centrifuged at 800 RCF for 15 min and the supernatant discarded. The pellet was resuspended in the same buffer, protein content determined via Nanoquant Proteinassay (Carl Roth, Karlsruhe, Germany) in a Plate Reader (FluoStar Optima, BMG Labtech, Ortenberg, Germany), and the suspension finally diluted to 30 mg protein/ml.

The knockout of AQP5 in the mice was verified by Western blotting as described in (18). SDS-PAGE was performed on a 1-mm-thick 9% acrylamide gel in a Mini-Protean 3 SDS-PAGE chamber (Bio-Rad). Samples were mixed 1:2 with sample buffer (130 mM Tris-HCl, 20% glycerol, 4.6% SDS, 0.02% bromphenol blue, and 2% DTT) and heated to 40°C for 5 min. This mixture was loaded onto the gel (15 µl/lane resulting in 15µg protein per lane). A Trans-Blot SD semidry transfer cell (Bio-Rad, Richmond, CA, USA) was used with a nitrocellulose membrane. Immunodetection was achieved with the AQP-5 antibody (affinity-purified polyclonal antibody against the murine/rat AQP-5 C-terminal region (245-265aa) (Biozol Diagnostica, Eching, Germany) and, as secondary antibody, anti-rabbit-IgG IRDye680CW (Li-Cor Biosciences, Lincoln, NE, USA). The Odyssey Infrared Imaging System (Li-Cor Biosciences) was used for visualization of the antibody-labelled protein bands. Fig. 1 confirms that in the lungs of the mice used here AQP5 (mol.wt. ~ 27 kDa (29)) was present in WT and absent in KO animals.

Maximal O_2 consumption by the Helox technique.- These measurements were done on conscious mice using the Helox technique (5, 30) as described by us earlier (1). Before performing the measurements of $\dot{V}_{O2max}$ (and of arterial oxygen saturation, S_{O2}, (see below)), the animals were acclimatized to the cold by exposure for 5 hrs. per day over 4 weeks to 4°C in the cold room (31). As we had ascertained earlier (1), this led, due to a substantial increase in brown adipose tissue (BAT)(31), to a prolonged perseverance of the animals under the conditions of the $\dot{V}_{O2max}$ and S_{O2} measurements with 79% He in the inspired gas at 4°C (see below). This longer perseverance helped to establish stable plateau values in both measurements, indicating that the animals' metabolism had reached a steady state. A gas reservoir in a cold room (4°C) was flushed by a mixture of 79% He with 21% O_2 (normoxic) or of 79% He with 11% O_2 and 10% N_2 (hypoxic) precooled to 4°C and saturated with water vapor at this temperature before entering the reservoir. A respiratory box (inner dimensions 8 x 7 x 13 cm), in which a mouse was placed, was perfused at a defined flow rate of ~ 35 l/h with gas from the reservoir. We note that at the dimensions given, the high diffusivity of O_2 in air alone ensures the near absence of O_2 gradients within this chamber. The outflowing gas was dried and then led through a mass flow meter (Fig. 1 in ref.(1)). Part of the gas flowing out of the flow meter was pumped into a FoxBox oxygen analyzer (FoxBox; Field Oxygen

Analysis System; Sable Systems, North Las Vegas, NV 89032 USA). The same Fig. 1 in (1) shows that in parallel an identical flow of the same gas mixture was established through an empty reference box (with identical dimensions), which was also dried before flow and O_2 concentration were measured. From the (dried) gas flow leaving the respiratory box and the O_2 concentrations in the (dried) gas mixtures flowing out of the respiratory and the reference box, respectively, the animal's oxygen consumption was calculated using eq. 11.2 (on p. 126 of (32)):

$$\dot{V}_{O2,max} = FR_e\,(F_{iO2} - F_{eO2}) \,/\, [1 - F_{iO2}\,(1 - RQ)],$$

where FR_e is the flow rate out of the respiratory box after drying, F_{iO2} is the O_2 concentration of the gas flowing out of the reference box, F_{eO2} is the O_2 concentration of the gas flowing out of the respiratory box (both after drying), and RQ is the respiratory quotient. With regard to the latter, we note that simultaneous measurement of CO_2 in the FoxBox was not possible because of a drastic and persisting drift of the CO_2 sensor's baseline in the presence of He at 4°C. Thus, the respiratory quotient RQ could not be determined here. The results for $\dot{V}_{O2,max}$ given below were calculated for the average RQ=0.8. If at normoxia the RQ value were assumed to be 1.0, the $\dot{V}_{O2,max}$ values given here would decrease by $\sim$4%, with RQ=0.7 they would increase by $\sim$2%. These latter two percentages indicate the maximal degree of uncertainty in the present $\dot{V}_{O2,max}$ determinations due to lack of knowledge of the actual RQ value, an uncertainty of minor significance in view of the differences between WT- and KO-mice seen in Fig. 3.

In the present experiments, the Helox measurement was continued until a stable plateau of $\dot{V}_{O2,max}$ was reached. A plateau value was usually reached after a few minutes and the experiment was then continued for several more minutes to ascertain the stability of this plateau, and measurement was taken from the entire plateau. After $\dot{V}_{O2,max}$ began to decline after the plateau phase, we found that body temperature of the animals also began to decline after having been stable during the plateau phase. All $\dot{V}_{O2,max}$ values are given per body weight, as specific oxygen consumptions.

It has been shown by Rosenmann and Morrison and several others (4–6) that the maximal increases in oxygen consumption over the resting level seen by Helox under cold exposure are under many conditions about identical to the

increases seen under treadmill or wheel running. It should be noted, however, that a divergence between exercise- and cold-induced $\dot{V}_{O2,max}$ values has been reported especially in mice cold-acclimatized for the extremely long time of 9 weeks at 5°C, which then exhibited a 60% greater thermogenic capacity in the cold than under exercise (33–35).

Lung parameters.- Lung function was characterized on mice anesthetized with ketamine-xylazine and then tracheostomized and cannulated before being analyzed using a forced pulmonary maneuver system (36) (Buxco Research Company, Data Sciences International) running FinePointe Software (version 6, Data Sciences International). A breathing frequency of 150 breaths/min was imposed on the anesthetized animals. The quasistatic PV maneuver protocol was followed to determine vital capacity (VC) and residual volume (RV). The fast flow volume maneuver was followed to determine peak expiratory flow (PEF). Dynamic compliance (Cdyn) and inspiratory resistance (RI) were also determined. At least three maneuvers were performed per mouse and the mean value taken. The CO diffusion factor DF_{CO} of lungs (a quantity closely related to the CO diffusing capacity DL_{CO}) was determined using a small concentration of CO plus a low concentration of Ne as an insoluble tracer gas in the inspired gas mixture. The principle was as described earlier (37). 0.8 ml mixed gas (0.5 % Ne, 21 % O_2, 0.5 % CO and 78 % N_2) was instilled into the mice lungs through the cannula and withdrawn 2 s later for analysis on a 3000 Micro GC Gas Analyzer (Infinicon) running EZ IQ software v3.3.2 (Infinicon). DF_{CO} was calculated as 1-(CO1/CO0)/(Ne1/Ne0) where 0 and 1 refers to the gas concentration before and after instillation respectively. DF_{CO} is a dimensionless quantity varying between 0 and 1, where 0 represents no uptake of CO at all, and 1 a complete uptake of all CO. In addition to the functional parameters we determined morphological parameters from hematoxylin-eosin- (HE) -stained lung tissue sections as described previously (38), especially mean chord length, MCL, as an indicator of emphysema, and we observed the number and size of inflammatory infiltrations.

Arterial S_{O2} and heart rate by pulse oximetry under conditions of maximal O_2 consumption.- Arterial oxygen saturations in the carotid artery (S_{O2}) as well as heart rates (HR) were measured in conscious animals with a MouseOX Plus

pulse oximeter (Starr Life Sciences Corp., Oakmont, PA 15139 USA) using ThroatClip sensors size M or S, depending on animal size. Further details were as described earlier (1). The S_{O2} and HR measurements were performed under conditions identical to those of the $\dot{V}_{O2,max}$ determinations, under normoxia or hypoxia in the He-O_2-(N_2-) flushed respiratory box at 4°C. Also, mice had been pre-acclimatized to 4°C as described for $\dot{V}_{O2,max}$ measurements. After several minutes a plateau was reached for S_{O2} and HR, and the values of this plateau were used in Table 1. Due to the initial agitation of the animals right after placement in the respiratory box, the initial HR values were even higher than those of the plateau.

Development of brown adipose tissue in response to intense cold exposure.- Again, a *cold acclimatization* protocol was performed whose effect on the amount of interscapular brown adipose tissue (iBAT) had been quantitated earlier (39) and found to yield about identical increases in iBAT as the protocol described above for the preparation of the animals for $\dot{V}_{O2,max}$ determination (31). Six female wild type and six female AQP5 knockout mice where housed individually in standard makrolon cages type 3 on wood shaving substrate with water and food (Altrumin 1324 TPF maintenance diet) ab libitum in a 12:12 hrs. light cycle. All animals where in the same age and body weight range. Animals were first exposed to 16°C for two weeks, followed directly by 24 hrs./day exposure to 4°C for additional two weeks. Body weight was controlled at the beginning, after the first and the second two-week periods. After the last adaptation period, animals where sacrificed via cervical dislocation and iBAT was removed, separated from surrounding white adipose tissue and weighed. *Preparation of BAT cells* was performed after (40). iBAT was again cut out from the cold-adapted mice, and surrounding white adipose and connective tissue were removed. Isolation of iBAT cells was achieved by a modification of the protocol of Pettersson and Vallin (40). In short: the mass of the extracted iBAT was determined for each individual mouse and the BAT from 3 animals was then pooled for one cell preparation. The pooled BAT was finely minced with scissors in an 1.5 ml plastic tube containing 3 ml/g tissue of a modified Krebs-Ringer phosphate buffer (110.9 mM NaCl, 1.4 mM KH_2PO_4, 3.8 mM NaH_2PO_4, 16.7 mM Na_2HPO_4, 1.5 mM $CaCl_2$, 10 mM glucose, 10 mM fructose, 4% bovine serum albumin and 2 mg/ml collagenase). The tissue suspension was incubated for 5 min in a 37°C water bath and vortex-stirred every 60 seconds.

The suspension was layered onto a 100 µm cell strainer and washed with 5 ml buffer. The tissue was then removed from the strainer and incubated for additional 30 min at 37°C in the same buffer, with vortex stirring every 5 minutes. After complete digestion, the tissue suspension was filtered through a 100 µm cell strainer and washed 3 times in buffer without collagenase by centrifugation at 1000g for 10 min and resuspension. The resulting cell pellet was carefully re-suspended in 300 µl buffer without collagenase, leaving the denser lowest pellet of red blood cells behind. The red cell pellet was discarded. Number of brown adipose cells was then determined with a Neubauer counting chamber. Cytochrome c contents of these cells were determined using the Quantikine ELISA Rat/Mouse Cytochrome C kit from R&D Systems and FLUOSTAR Optima Plate reader (BMG Labtech, Ortenberg, Germany). Cellular protein concentration was determined by Bradford ROTI Nanoquant (Carl Roth, Karlsruhe, Germany). Uncoupling protein-1 (UCP1) in the same cells was quantitated after cell lysis by the Uncoupling Protein 1 BioAssay ELISA Kit (Mouse) (USBiological, Life Sciences, Cat.No. 028766; Salem MA, USA). The assay was performed in the above plate reader using an absorbance wavelength of 450 nm.

Results

Maximal O_2 consumption of AQP5-KO and WT mice in normoxia and hypoxia.- Fig. 2a and b show the measured specific $\dot{V}_{O2,max}$ values for wild type mice under normoxia and hypoxia (11% O_2, corresponding to an altitude of about 4500 m). The values seen in Fig. 2a agree well with those reported previously for various other Bl/6 wild type mice (1, 5, 6). Also, the values seen under hypoxia in Fig. 2b are about 40% lower than the normoxic $\dot{V}_{O2,max}$ values, which agrees with the hypoxic values reported earlier (1). Comparing female (red dots) and male (grey dots) mice, it is apparent from both data sets that sex has no major effect on $\dot{V}_{O2,max}$, except by the lower body weight of females compared to males. This is in agreement with the minimal effect of sex on $\dot{V}_{O2,max}$ seen previously in cold-adapted animals (41). The regression lines with fairly good correlation coefficients of Fig. 2 a and b thus allowed us to describe the dependency of $\dot{V}_{O2,max}$ on body weight in WT under normoxia and hypoxia. The fact that the specific $\dot{V}_{O2,max}$ values of WT in Figs. 2a and b decrease with increasing body weight is at least partially explained by the fact that body surface is an important determinant of $\dot{V}_{O2}$ and increases with increasing body

weight to lesser extent than body weight itself. In other words, the slopes in both figures reflect the fact that surface-to volume ratio decreases with increasing body weight (42, 43).

It is apparent from Figs. 2c and d that the body weights of the Aqp5 $^{-}/^{-}$ mice tend to be lower than those of wild type mice. In order to identify the important variable(s) determining the resulting values of $\dot{V}_{O2,max}$, we used a multiple regression analysis (IBM SPSS Statistics, Version 21) with the numerical dependent variable $\dot{V}_{O2,max}$, the numerical independent variable body weight, and the two nominal dummy-coded independent variables sex and genotype. The result shows that in both, the sets of data at normoxia and hypoxia, sex is not a significant influence (p= 0.20 and p= 0.56, respectively). This is quite compatible with the appearance of the data of Fig. 2. Again in line with the appearance of the data in Fig. 2, body weight has a significant influence on $\dot{V}_{O2,max}$ in normoxia (p=0.004) but a lesser one in hypoxia (p=0.08). The analysis, on the other hand, shows clearly that genotype constitutes the decisive influence on $\dot{V}_{O2,max}$ both in normoxia (p=0.003) and in hypoxia (p=0.001). The latter p-values suggest that the dependence on genotype may even be somewhat greater in hypoxia than in normoxia, an observation compatible with the graphical representation of the data given in Fig. 3 (see below). We conclude that genotype is the major influence on the value of $\dot{V}_{O2,max}$ and the differences in $\dot{V}_{O2,max}$ between WT and KO animals are highly significant.

In order to visualize the effects on $\dot{V}_{O2,max}$ by genotype, body weight and sex, we used the slopes of the regression lines for WT shown in Fig. 2a and b in order to correct all female and male WT $\dot{V}_{O2,max}$ values, respectively, to the average body weights of the corresponding female and male KO groups in Fig. 2c and d (the averages of the KO groups are shown by the big dots in both latter figures for the case of each (separately considered) sex). The body-weight-corrected WT data are then shown in Fig. 3 as columns on the left-hand sides in comparison to the KO data for identical body weights (on the right hand sides). The appropriate body weight is given at the bottom of the figure for each pair of columns. To obtain an impression of the level of significance for each of these individual comparisons, unpaired t tests (GraphPad Prism 6) were applied to the groups of WT vs. KO values for all conditions of Fig. 3. The results are shown in the figure in terms of percent difference between WT and KO and in terms of the level of significance of this difference (number of stars). As

expected, these results are consistent with the general results of the multiple regression analysis. Combining male and female data ("all data") we find a reduction of $\dot{V}_{O2,max}$ in KO animals under normoxic conditions by 21% and under hypoxic conditions by 26% (left hand panel in Fig. 3). Considering male and female data separately (right hand panel in Fig. 3), we observe reductions in all KO groups, although the reduction is smallest and statistically not significant in male normoxic animals (13%), but greater and statistically significant in male hypoxic data (19%), and in female normoxic (28%) and hypoxic data (34%). Overall, it is clear that $\dot{V}_{O2,max}$ in AQP5-KO animals is markedly reduced by up to 1/3. It may also be noted that the differences are more pronounced and reach higher levels of statistical significance under hypoxia than under normoxia, in agreement with the multiple regression analysis.

Parameters of lung function in AQP5-KO and WT mice.- Fig. 4 shows the results of the standard lung function parameters vital capacity, VC, residual volume, RV, dynamic compliance, C_{dyn}, inspiratory resistance, Ri, and peak expiratory flow, PEF. In a two-way ANOVA with Sidak's multiple comparison test, almost all these values show no significant difference between WT and KO animals, both in females and in males. The exception is DF_{CO} in females, which shows a weakly significantly greater DF_{CO} in KO vs. WT animals. Of course also this latter observation argues clearly against a significant role of AQP5 as an O_2-conducting pathway. In agreement with this finding on DF_{CO}, a two-way ANOVA with interaction test shows only in the case of DF_{CO} a (weakly) significant interaction between the effects of gender and genotype on lung parameters (see legend to Fig. 4). Although male KO animals show a slightly elevated score for emphysema on the basis of the mean chord length, MCL, as observed in lung tissue sections (Figs. S1, S2a; Supplemental Figures https://doi.org/10.6084/m9.figshare.20097401.v2), and female KO animals show a somewhat elevated score for inflammation, as determined from the number and size of inflammatory foci seen in tissue sections (Fig. S2b; Supplemental Figures https://doi.org/10.6084/m9.figshare.20097401.v2), none of these differences is statistically significant. In the case of MCL, this agrees with Aggarwal et al. (26), who find no difference in MCL between WT and AQP5-KO mouse lungs exposed to air (although these authors do find an increase in MCL of WT but not of KO after the animals had been exposed to cigarette smoke). These findings are compatible with the lung function

parameters given in Fig. 4, which show in no case a significant difference between WT and KO animals that would indicate that absence of AQP5 might impair pulmonary uptake of O_2. This allows us to conclude that there are no differences in lung volumes, compliance, elasticity and airway resistance between WT and KO. We note that induction of lung emphysema by oropharyngeal aspirations of elastase (38) induced a marked increase in emphysema score, but this happened quantitatively similarly in WT and KO mice (Fig. S3; Supplemental Figures https://doi.org/10.6084/m9.figshare.20097401.v2). With respect to the main aim of the present paper, the last panel of Fig. 4 (DF_{CO}) represents an important finding showing the absence of a meaningful facilitation of gas transfer across the alveolar-capillary barrier by AQP5 in WT of both sexes.

Arterial S_{O2} under conditions of normoxic and hypoxic maximal O_2 consumption.- In order to ascertain whether oxygen uptake in the lung is potentially limited in AQP5-KO mice under conditions of $\dot{V}_{O2,max}$, we measured carotid arterial oxygen saturation in these conditions. Table 1 gives the results for S_{O2} together with the associated values of heart rates. It is apparent that arterial S_{O2} under normoxia is normal at 98% both in WT and KO animals. This shows that in both types of mice there is no pulmonary limitation of O_2 uptake. Under hypoxia at an inspiratory O_2 concentration of 11%, arterial S_{O2} was 72%, a value intermediate between the S_{O2} of 55% observed at hypobaric hypoxia equivalent to an inspiratory O_2 concentration of 10.5% under maximal aerobic exercise in rats (44), and the value of 77% observed at the higher inspiratory O_2 concentration of 13.5 % under high-intensity interval exercise in humans (45). Again, it is apparent that S_{O2} is identical in WT and KO animals, indicating that lack of AQP5 in pulmonary epithelium does not cause a noticeably impaired O_2 equilibration across the alveolo-capillary barrier in hypoxia, as it does not in normoxia.

Mass and properties of BAT after intense acclimatization of KO and WT mice to cold.- We find here that during the 4 weeks of two 24 h-per-day phases of acclimatization to two grades of cold, AQP5-KO mice form substantially less interscapular brown adipose (iBAT) tissue than WT mice. Table 2 shows first that neither during the two weeks of acclimatization to 16°C nor during the subsequent two weeks of acclimatization to 4°C is there any change in body

483 weight of the animals. Also, there is no difference in body weights between KO
484 and WT animals. However, the absolute weight of the excised iBAT is 120 mg in
485 KO mice and with 157 mg about 30% greater in WT mice. The same holds for
486 the iBAT weights per body weight, which are 4.88 mg/g in KO mice and 6.28
487 mg/g in WT mice, i.e. 29% greater in WT. In mice without cold adaptation we
488 find iBAT masses of 3.97 (± 0.93 SD, n=5) mg/g for WT animals and of 3.91 (±
489 0.56 SD, n=5) mg/g for KO animals. Thus, in non-acclimated animals there is no
490 difference in iBAT mass between KO and WT (ns in an unpaired t-test with
491 p=0.92). However, under intense cold exposure iBAT mass in WT mice increases
492 by 63% from 3.97 to 6.28 mg/g, while in KO mice it increases only by 25% from
493 3.91 to 4.88 mg/g. Thus, the increase in brown adipose tissue in response to an
494 intense cold stimulus is 2.5-fold greater in WT than in AQP5-KO animals.
495 *Cytochrome c content* as an indicator of mitochondrial density was determined
496 to be 800 ng and 700 ng per $1 \cdot 10^6$ isolated WT BAT cells in two pools of cells
497 (each of them pooled from three WT animals), and, in the case of AQP5-KO
498 animals, 719 ng and 588 ng per $1 \cdot 10^6$ isolated BAT cells from two cell pools.
499 Clearly, there is no drastic difference in cytochrome c content of both types of
500 cells. However, all values are at least 10 times higher than one finds with this
501 cytochrome assay in non-BAT cells (17 – 63 ng per $1 \cdot 10^6$ cells according to the
502 supplier of the kit). These cytochrome c values can be compared with the
503 literature, when they are divided by the cellular protein concentrations. For the
504 present data, this gives 110 and 75.1 pmol cytochrome c/mg protein for the
505 two WT cell pools, and 91.2 pmol/mg and 95.6 pmol/mg for the two AQP5-KO
506 cell pools. These numbers compare reasonably with the figure of 153 pmol/mg
507 reported for brown adipocyte tissue after an even more extended cold
508 exposure of the animals than ours (46). *Determinations of UCP1 contents* in the
509 same four cell preparations just mentioned yielded 565 ng and 799 ng per
510 $1 \cdot 10^6$ isolated WT BAT cells, and 409 ng and 694 ng per $1 \cdot 10^6$ isolated BAT cells
511 from AQP5-KO animals. It turns out that like in cytochrome c contents, there is
512 no major difference in UCP1 concentrations between iBAT cells from WT and
513 KO animals.

514 In conclusion, interscapular BAT mass after intense cold exposure is
515 significantly lower in AQP5-KO than in WT mice. However, we find no major
516 difference in cytochrome c concentration between BAT from AQP5-KO and WT
517 mice, and both cytochrome c concentrations agree reasonably well with the

518 literature. Also, UCP1 as an indicator of BAT activation is similar in BAT cells
519 from AQP5-KO and WT animals.

520

521 **Discussion**

522 **Reduced maximal body oxygen consumption of AQP5-KO mice by the Helox**
523 **technique.-** The Helox technique is an accepted method to determine maximal
524 oxygen consumption of small animals. As stated above, it produces often the
525 same increases of $\dot{V}_{O2}$ as they are seen by maximal physical activity under
526 forced wheel running (5, 6)**.** However, after severe cold acclimatization, $\dot{V}_{O2,max}$
527 determined by the Helox method may be greater than that determined by
528 maximal exercise (33–35). Nevertheless, the $\dot{V}_{O2,max}$ values of WT mice seen
529 under normoxia (Fig. 2) are identical to those reported by both techniques in
530 the literature for mice in normoxia (1, 5, 6). Similarly, the $\dot{V}_{O2,max}$ values seen in
531 Fig. 2 under hypoxia agree well with those reported previously under identical
532 conditions (1).

533 The novel result of the multiple regression analysis described above and of Fig.
534 3 is the observation of a reduction of $\dot{V}_{O2,max}$ in AQP5-KO animals by up to 34%,
535 the number obtained for female mice under hypoxic conditions. However,
536 major reductions are also seen in Fig. 3 for female mice in normoxia and for
537 males in hypoxia. We conclude that the absence of AQP5 decreases either the
538 uptake of O_2 in the lung or the transport of O_2 into tissues.

539 Is it conceivable that AQP5 acts as a transport route of O_2 through cell
540 membranes? No direct evidence has been presented so far for such an effect.
541 However, two other aquaporins with properties similar to those of AQP5, AQP1
542 and AQP4, have been shown by experimental approaches (14, 15) and by
543 molecular dynamics (MD) simulations to conduct O_2 in addition to CO_2 (9, 13).
544 In addition, recently AQP5 has been shown by MD and by expression of AQP5
545 in oocytes to be a good pathway for CO_2 (7, 8). This makes it conceivable that
546 AQP5 might also conduct O_2, most likely in the central pore of the tetramer.

547 In which organs could AQP5 facilitate O_2 transport across cell membranes?
548 AQP5 has been found to a major extent in the lung, bronchi, trachea, salivary,
549 parotid and lacrimal glands, and the eye (22, 24, 47, 48). Most of these organs
550 are too small to affect whole body $\dot{V}_{O2}$ significantly. However, the lung is the

largest one of these organs and by far the one with the greatest fluxes of O_2 occurring across its membranes. It is relevant in this context that Nielsen et al. (20) have shown that in the lung AQP5 is localized to the apical plasma membrane of type I pneumocytes, which cover the majority of the surface of the alveoli. Thus, we formulated the tentative hypothesis that AQP5 in this membrane might accelerate the flux of O_2 across the alveolar-capillary barrier and thus facilitate O_2 uptake by the lung. To study this possibility, we investigated lung function and arterial oxygen saturation.

Does an impaired oxygen uptake in the lung of AQP5-KO mice reduce maximal oxygen consumption? – As shown above, we have done a thorough investigation of many lung functional parameters and found practically all of them to be normal. This finding is in excellent agreement with the observations of Krane et al. (25) on airway resistance, dynamic compliance and airway pressure time index, which were identical between KO and WT mice at low concentrations of acetylcholine. Also, it agrees with Aggarwal et al. (26), who found no evidence for signs of emphysema in KO mice. Most interesting in the present context is the pulmonary diffusion factor DF_{CO}, which describes the global diffusion properties of the lung of WT and KO mice. There is clearly no reduction of DF_{CO} in AQP5-KO mice, neither in females nor in males. It should be noted that DF_{CO}, for methodological reasons, uses CO rather than O_2 as the diffusing gas (37). It is not known, whether aquaporins conduct CO as well as O_2, although this may be expected in view of the smaller size of CO. Thus, there is evidence against a role of AQP5 in O_2 diffusion across the alveolar-capillary barrier, although it may not be considered entirely conclusive. We have therefore in addition studied the arterial oxygen saturation in the carotid artery, which reflects the degree of equilibration of lung capillary blood with alveolar O_2 partial pressure. Table 1 shows that AQP5-KO as well as WT mice achieve under normoxia an identical and entirely normal arterialization of about 98%. Also under hypoxia, where an arterial oxygen saturation of 72% is achieved, there is no difference between KO and WT animals. Moreover, this saturation agrees very well with the saturation reported by Gonzalez et al. (44) for resting rats under a similar level of hypoxia. Thus, neither the diffusion capacity of the lungs nor the arterial oxygen saturations suggest any crucial role of AQP5 in pulmonary blood oxygenation. The alveolo-capillary barrier, which is as thin as 0.5 – 1 µm, either is not increased in its O_2 conductivity by AQP5, or

its conductivity is so high that functionally it does not require a further increase by AQP5. A similar conclusion has been reached for the case of CO_2 conduction across the alveolo-capillary barrier from studies of artificially perfused lungs by Swenson et al. (49).

In conclusion, the lack of AQP5, which causes a marked reduction of maximal $\dot{V}_{O2}$, does not do so by an impaired pulmonary O_2 uptake. The only alternative explanation then seems to be an impaired oxygen consumption of an intensely O_2-consuming peripheral organ.

AQP5 deficiency impairs development of brown adipose tissue under cold acclimatization.- The enhanced oxygen consumption during cold exposure is in several species mainly generated by brown adipose tissue, skeletal muscle when shivering occurs, and by the elevated activity of heart and respiratory muscles (50). In many cases, BAT contributes the majority of the increase in $\dot{V}_{O2}$ under cold exposure (50). A further argument for favoring BAT as a candidate for the AQP5-dependent increase in $\dot{V}_{O2,max}$ is the lack of AQP5 expression in rat skeletal muscle and heart (22), while on the other hand more recently a markedly higher expression of AQP5 in BAT compared to white adipose tissue has been observed (23). This was the motivation to study the mass of interscapular BAT (iBAT) and the properties of isolated brown adipocytes in intensely cold-acclimated AQP5-KO and WT mice.

Table 2 shows that indeed the development of BAT under cold exposure is markedly inhibited in AQP5-KO compared to WT mice. Whereas WT mice have 157 mg of interscapular BAT after the four weeks of graded cold adaptation, AQP5-KO mice possess only 120 mg. The increase in specific iBAT mass by the cold exposure was 63% in WT mice, but only 25% in AQP5-KO mice. While KO mice develop significantly less iBAT, the cytochrome c content of the BAT cells that are present is similar in WT and KO mice, and likewise are the concentrations of UCP1 in BAT cells similar in WT and KO. This indicates that the mitochondrial density within the available BAT cells is about equal in both situations, and their capacity for non-shivering thermogenesis should also be about equal. A weight of 120 mg iBAT is normal in Bl/6 mice kept at 30°C, a weight of 157 mg is also normal in Bl/6 mice kept for a prolonged time at 4°C ((51), Fig. 2B). This would indicate that the BAT mass shown in Table 2 for WT mice is normal after cold acclimatization, while the value observed for AQP5-

KO mice reflects a drastically diminished response to the cold exposure. Madeira et al. (52), using the 3T3-L1 preadipocyte cell line, observed an impairment of adipocyte differentiation when the expression of AQP5 was suppressed. We conclude that the expression of AQP5 is crucial for the transformation of white to brown adipose tissue under cold exposure. BAT has recently come into focus as an important beneficial factor regulating glucose and lipid metabolism also in humans (53). For example, it has been shown that in adipose men with type 2 diabetes BAT is "whitened" and shows a reduced glucose uptake (54). Thus, the metabolic situation of these individuals would improve if their BAT could be made to increase. In such a transformation, AQP5 will obviously play an important role.

What is the cause of the reduction of $\dot{V}_{O2,max}$ of AQP5-KO mice? In normal mice $\dot{V}_{O2,max}$ is limited by the capacity of the cardio-respiratory system. Enhanced exercise capacity is often associated with enhanced stroke volume and cardiac output, besides adaptations in the skeletal muscle system. For this reason, $\dot{V}_{O2,max}$ is in many cases identical whether the increase in $\dot{V}_{O2}$ is caused by forced wheel or treadmill running or by increased non-shivering thermogenesis under cold exposure. A reduction of $\dot{V}_{O2,max}$ by the cardiorespiratory system is unlikely to apply in AQP5-deficient animals, because AQP5 is not involved in pulmonary gas exchange function, as shown in this paper, and because it is not expressed in the heart (22). Likewise, a role of skeletal muscle in the reduction of $\dot{V}_{O2,max}$ is not expected because AQP5 is also not expressed in skeletal muscle (22). This gives rise to the hypothesis that it is the reduction of the mass of iBAT (and possibly further BAT depots) that limits the increase in $\dot{V}_{O2,max}$ of AQP5-KO animals, when the Helox technique is used to determine this parameter. With the data available, therefore, we conclude that in cold-acclimated AQP5-KO mice the significant reduction of BAT by ~25% leads to the reduction of $\dot{V}_{O2,max}$ by around 25%. This quantitative coincidence suggests a causal relationship between changes in $\dot{V}_{O2,max}$ and iBAT. It might be added that the observed reduction of iBAT presumably applies similarly to the other localizations of BAT.

Although the details of the cold acclimatization protocols used for the $\dot{V}_{O2,max}$ measurements and the iBAT weight determinations were – for technical reasons – not identical, the above conclusion is obvious, because both protocols lead to similar and substantial increases in BAT mass (31, 39). While

this result must not exclude a role of AQP5 as an O_2 channel in adipocytes during their transformation into brown adipocytes, it provides no explicit evidence for such a function. Alternatively, AQP5 might be involved in this transformation process in some other way, e.g. by mediating cellular water fluxes or by its interaction with the transient receptor potential vanilloid 4 (TRPV4) as has been proposed (52, 55). It might also act in a fashion similar to the role of AQP1 in migration and proliferation of several cell types such as for example in pulmonary vascular cells (56).

Perspectives and Significance

This paper presents three major observations: 1) maximal body O_2 consumption, $\dot{V}_{O2,max}$, elicited by cold exposure of mice acclimatized to the cold, is reduced by 20-30% in AQP5 knockout (KO) mice, 2) this reduction is not due to a limitation in the animals' O_2 uptake in the lung, since the lung diffusion factor as well as arterial O_2 saturation are identical between wild-type and KO mice, and 3) the reduced $\dot{V}_{O2,max}$ is likely due to the brown adipose tissue (BAT) in KO mice, whose mass is reduced by 25% compared to wild-type. Observation 3 is consistent with the fact that under cold exposure a majority of the increase in $\dot{V}_{O2,max}$ observed in acclimatized animals is generated by the enhanced mass of intensely metabolizing BAT. Thus, we report here the novel findings that a) AQP5 – although it is a putative gas channel and strongly expressed in pulmonary epithelium – does not contribute to O_2 uptake in the lung, but b) AQP5 instead is vital for the conversion of white into brown adipose tissue under acclimatization to the cold. The role of AQP5 in this latter process represents an exciting starting point for the study of the mechanism of this conversion. Understanding and exploiting this mechanism will have great therapeutic potential in the context of attempts to improve the metabolic situation in type 2 diabetes and metabolic syndrome, which is known to be positively affected by BAT.

Acknowledgment.- We thank the Deutsche Forschungsgemeinschaft for financial support of this work (project EN 908/3-1) and the German Federal Ministry of Education and Research (Infrafrontier grant 01KX1012 to MHdA)

Data Availability. The data of this study are available from the authors upon request.

Conflict of interest.- The authors declare no conflict of interest.

Author Contributions.- Concept of study: GG, VE, SA-S; Breeding, genotyping and characterization of animals in Baltimore VKS, LSK and in Hannover SA-S, VE; Cold acclimatization, $\dot{V}_{O2,max}$ and BAT measurements SA-S, VE, GB; Lung function parameters AÖY, TMC, CS and phenotyping conceptualization and supervision VG-D, HF, MHdA; Data evaluation SA-S, VE, GG, AÖY, TMC, VD-D, HF; Funding acquisition VE, MHdA; 1st draft of manuscript GG, VA-S, VE. All authors have critically read the manuscript, suggested improvements and agreed to the final version.

References

1. **Al-Samir S**, **Goossens D**, **Cartron JP**, **Nielsen S**, **Scherbarth F**, **Steinlechner S**, **Gros G**, **Endeward V**. Maximal oxygen consumption is reduced in aquaporin-1 knockout mice. *Front Physiol* 7: 1–8, 2016. doi: 10.3389/fphys.2016.00347.

2. **Montiel V**, **Leon Gomez E**, **Bouzin C**, **Esfahani H**, **Romero Perez M**, **Lobysheva I**, **Devuyst O**, **Dessy C**, **Balligand JL**. Genetic deletion of aquaporin-1 results in microcardia and low blood pressure in mouse with intact nitric oxide-dependent relaxation, but enhanced prostanoids-dependent relaxation. *Pflugers Arch Eur J Physiol* 466: 237–251, 2014. doi: 10.1007/s00424-013-1325-x.

3. **Al-Samir S**, **Wang Y**, **Meissner JD**, **Gros G**, **Endeward V**. Cardiac morphology and function, and blood gas transport in aquaporin-1 knockout mice. *Front Physiol* 7: 1–22, 2016. doi: 10.3389/fphys.2016.00181.

4. **Segrem N**, **Hart J**. Oxygen supply and performance in Peromyscus. Comparison of exercise with cold exposure. *Can J Physiol Pharmacol* 45: 543–549, 1967. doi: 10.1139/y67-063.

5. **Rosenmann M**, **Morrison P**. Maximum oxygen consumption and heat loss facilitation in small homeotherms by He O2. *Am J Physiol* 226: 490–495, 1974. doi: 10.1152/ajplegacy.1974.226.3.490.

6. **Chappell MA**. Maximum oxygen consumption during exercise and cold exposure in deer mice, Peromyscus maniculatus. *Respir Physiol* 55: 367–

377, 1984. doi: 10.1016/0034-5687(84)90058-6.

7. **Geyer RR**, **Musa-Aziz R**, **Qin X**, **Boron WF**. Relative CO2/NH3 selectivities of mammalian aquaporins 0-9. *Am J Physiol - Cell Physiol* 304: C986–C994, 2013. doi: 10.1152/ajpcell.00033.2013.

8. **Alishahi M**, **Kamali R**. A novel molecular dynamics study of CO2 permeation through aquaporin-5. *Eur Phys J E* 42, 2019. doi: 10.1140/epje/i2019-11912-x.

9. **Wang Y**, **Cohen J**, **Boron WF**, **Schulten K**, **Tajkhorshid E**. Exploring gas permeability of cellular membranes and membrane channels with molecular dynamics. *J Struct Biol* 157: 534–544, 2007. doi: 10.1016/j.jsb.2006.11.008.

10. **Endeward V**, **Musa-Aziz R**, **Cooper GJ**, **Chen L -M. M**, **Pelletier MF**, **Virkki L V.**, **Supuran CT**, **King LS**, **Boron WF**, **Gros G**. Evidence that aquaporin 1 is a major pathway for CO2 transport across the human erythrocyte membrane. *FASEB J* 20: 1974–1981, 2006. doi: 10.1096/fj.04-3300com.

11. **Musa-Aziz R**, **Chen LM**, **Pelletier MF**, **Boron WF**. Relative CO 2/NH 3 selectivities of AQP1, AQP4, AQP5, AmtB, and RhAG. *Proc Natl Acad Sci U S A* 106: 5406–5411, 2009. doi: 10.1073/pnas.0813231106.

12. **Nakhoul NL**, **Davis BA**, **Romero M**, **Boron W**. Effect of expressing the water channel aquaporin-1 on the CO2 permeability of Xenopus oocytes. *Am J Physiol* 274: C543–C548, 1998. doi: 10.1152/ajpcell.1998.274.2.c297.

13. **Wang Y**, **Tajkhorshid E**. Nitric oxide conduction by the brain aquaporin AQP4. *Proteins Struct Funct Bioinforma* 78: 661–670, 2010. doi: 10.1002/prot.22595.

14. **Zhao P**, **Geyer RR**, **Salameh AI**, **Wass AB**, **Taki S**, **Huffman DE**, **Meyerson HJ**, **Occhipinti R**, **Moss FJ**, **Boron WF**. Role of channels in the oxygen permeability of red blood cells. .

15. **Zwiazek JJ**, **Xu H**, **Tan X**, **Navarro-Ródenas A**, **Morte A**. Significance of oxygen transport through aquaporins. *Sci Rep* 7: 1–11, 2017. doi: 10.1038/srep40411.

16. **Boron WF**, **Endeward V**, **Gros G**, **Musa-Aziz R**, **Pohl P**. Intrinsic CO2 permeability of cell membranes and potential biological relevance of CO2 channels. *ChemPhysChem* 12: 1017–1019, 2011. doi: 10.1002/cphc.201100034.

17. **Dotson RJ**, **Pias SC**. Reduced oxygen permeability upon protein incorporation within phospholipid bilayers. *Adv Exp Med Biol* 1072: 405–411, 2018. doi: 10.1007/978-3-319-91287-5.

18. **Itel F**, **Al-Samir S**, **Öberg F**, **Chami M**, **Kumar M**, **Supuran CT**, **Deen PMT**, **Meier W**, **Hedfalk K**, **Gros G**, **Endeward V**. CO2 permeability of cell membranes is regulated by membrane cholesterol and protein gas channels. *FASEB J* 26: 5182–5191, 2012. doi: 10.1096/fj.12-209916.

19. **Al-Samir S**, **Itel F**, **Hegermann J**, **Gros G**, **Tsiavaliaris G**, **Endeward V**. O2 permeability of lipid bilayers is low, but increases with membrane cholesterol. *Cell Mol Life Sci* 78: 7649–7662, 2021. doi: 10.1007/s00018-021-03974-9.

20. **Nielsen S**, **King LS**, **Christensen BM**, **Agre P**. Aquaporins in complex tissues.II. Subcellular distribution in respiratory and glandular tissues of rat. *Am J Physiol - Cell Physiol* 273: C1549–C1561, 1997. doi: 10.1152/ajpcell.1997.273.5.c1541.

21. **King LS**, **Nielsen S**, **Agre P**. Aquaporins in complex tissues. I. Developmental patterns in respiratory and glandular tissues of rat. *Am J Physiol - Cell Physiol* 273: 1549–1561, 1997. doi: 10.1152/ajpcell.1997.273.5.c1541.

22. **Umenishi F**. Quantitative analysis of aquaporin mRNA expression in rat tissues by RNase protection assay. *DNA Cell Biol* 15: 475–480, 1996. doi: 10.1089/dna.1996.15.475.

23. **Lopes PA**, **Martins R**, **Da Silva IV**, **Madeira MS**, **Prates JAM**, **Soveral G**. Modulation of aquaporin gene expression by n-3 long-chain PUFA lipid structures in white and brown adipose tissue from hamsters. *Br J Nutr* 120: 1098–1106, 2018. doi: 10.1017/S0007114518002519.

24. **Krane CM**, **Melvin JE**, **Nguyen H Van**, **Richardson L**, **Towne JE**, **Doetschman T**, **Menon AG**. Salivary Acinar Cells from Aquaporin 5-deficient Mice Have Decreased Membrane Water Permeability and Altered Cell Volume Regulation. *J Biol Chem* 276: 23413–23420, 2001. doi: 10.1074/jbc.M008760200.

25. **Krane CM**, **Fortner CN**, **Hand AR**, **McGraw DW**, **Lorenz JN**, **Wert SE**, **Towne JE**, **Paul RJ**, **Whitsett JA**, **Menon AG**. Aquaporin 5-deficient mouse lungs are hyperresponsive to cholinergic stimulation. *Proc Natl Acad Sci U S A* 98: 14114–14119, 2001. doi: 10.1073/pnas.231273398.

26. **Aggarwal NR**, **Chau E**, **Garibaldi BT**, **Mock JR**, **Sussan T**, **Rao K**, **Rao K**,

Menon AG, **D'Alessio FR**, **Damarla M**, **Biswal S**, **King LS**, **Sidhaye VK**. Aquaporin 5 regulates cigarette smoke induced emphysema by modulating barrier and immune properties of the epithelium. *Tissue Barriers* 1: e25248, 2013. doi: 10.4161/tisb.25248.

27. **Gailus-Durner V**, **Fuchs H**, **Becker L**, **Bolle I**, **Brielmeier M**, **Calzada-Wack J**, **Elvert R**, **Ehrhardt N**, **Dalke C**, **Franz TJ**, **Grundner-Culemann E**, **Hammelbacher S**, **Hölter SM**, **Hölzlwimmer G**, **Horsch M**, **Javaheri A**, **Vetoslav Kalaydjiev S**, **Klempt M**, **Kling E**, **Kunder S**, **Lengger C**, **Lisse T**, **Mijalski T**, **Naton B**, **Pedersen V**, **Prehn C**, **Przemeck G**, **Racz I**, **Reinhard C**, **Reitmeir P**, **Schneider I**, **Schrewe A**, **Steinkamp R**, **Zybill C**, **Adamski J**, **Beckers J**, **Behrendt H**, **Favor J**, **Graw J**, **Heldmaier G**, **Höfler H**, **Ivandic B**, **Katus H**, **Kirchhof P**, **Klingenspor M**, **Klopstock T**, **Lengeling A**, **Müller W**, **Ohl F**, **Ollert M**, **Quintanilla-Martinez L**, **Schmidt J**, **Schulz H**, **Wolf E**, **Wurst W**, **Zimmer A**, **Busch DH**, **de Angelis MH**. Introducing the German Mouse Clinic: Open access platform for standardized phenotyping. *Nat Methods* 2: 403–404, 2005. doi: 10.1038/nmeth0605-403.

28. **Fuchs H**, **Aguilar-Pimentel J**, **Amarie OV**, **Becker L**, **Calzada-Wack J**, **Cho Y-L**, **Garrett L**, **Hölter SM**, **Irmler M**, **Kistler M**, **Kraiger M**, **Mayer-Kuckuk P**, **Moreth K**, **Rathkolb B**, **Rozman J**, **da Silva Buttkus P**, **Treise I**, **Zimprich A**, **Gampe K**, **Hutterer C**, **Stöger C**, **Leuchtenberger S**, **Maier H**, **Miller M**, **Scheideler A**, **Wu M**, **Beckers J**, **Bekeredjian R**, **Brielmeier M**, **Stöger T**, **Wolf E**, **Wurst W**, **Yildirim AÖ**, **Zimmer A**, **Gailus-Durner V**, **Hrabe de Angelis M**. Understanding gene functions and disease mechanisms: phenotyping pipelines in the German Mouse Clinic. *Behav Brain Res* 352: 187–196, 2018. doi: https://doi.org/10.1016/j.bbr.2017.09.048.

29. **Krane CM**, **Towne JE**, **Menon AG**. Cloning and characterization of murine Aqp5: Evidence for a conserved aquaporin gene cluster. *Mamm Genome* 10: 498–505, 1999. doi: 10.1007/s003359901030.

30. **Wang LCH**, **Peter RE**. Metabolic and respiratory responses during Helox induced hypothermia in the white rat. *Am J Physiol* 229: 890–895, 1975. doi: 10.1152/ajplegacy.1975.229.4.890.

31. **Heldmaier G**. The effect of short daily cold exposures on development of brown adipose tissue in mice. *J Comp Physiol* 98: 161–168, 1975.

32. **Lighton J**. Measuring Metabolic Rates: a Manual for Scientists. Oxford Scholarship online 2019, 2008.

33. **Chappell MA**, **Hammond KA**. Maximal aerobic performance of deer mice in combined cold and exercise challenges. *J Comp Physiol B Biochem Syst*

Environ Physiol 174: 41–48, 2004. doi: 10.1007/s00360-003-0387-z.

34. **McClelland GB**, **Lyons SA**, **Robertson CE**. Fuel use in mammals: Conserved patterns and evolved strategies for aerobic locomotion and thermogenesis. *Integr Comp Biol* 57: 231–239, 2017. doi: 10.1093/icb/icx075.

35. **McClelland GB**, **Scott GR**. Evolved Mechanisms of Aerobic Performance and Hypoxia Resistance in High-Altitude Natives. *Annu Rev Physiol* 81: 561–583, 2019. doi: 10.1146/annurev-physiol-021317-121527.

36. **Vanoirbeek JAJ**, **Rinaldi M**, **De Vooght V**, **Haenen S**, **Bobic S**, **Gayan-Ramirez G**, **Hoet PHM**, **Verbeken E**, **Decramer M**, **Nemery B**, **Janssens W**. Noninvasive and invasive pulmonary function in mouse models of obstructive and restrictive respiratory diseases. *Am J Respir Cell Mol Biol* 42: 96–104, 2010. doi: 10.1165/rcmb.2008-0487OC.

37. **Fallica J**, **Das S**, **Horton M**, **Mitzner W**. Application of carbon monoxide diffusing capacity in the mouse lung. *J Appl Physiol* 110: 1455–1459, 2011. doi: 10.1152/japplphysiol.01347.2010.

38. **Yildirim AÖ**, **Muyal V**, **John G**, **Müller B**, **Seifart C**, **Kasper M**, **Fehrenbach H**. Palifermin induces alveolar maintenance programs in emphysematous mice. *Am J Respir Crit Care Med* 181: 705–717, 2010. doi: 10.1164/rccm.200804-573OC.

39. **Heldmaier G**. Temperature adaptation and brown adipose tissue in hairless and albino mice. *J Comp Physiol* 92: 281–292, 1974.

40. **Pettersson B**, **Vallin I**. Norepinephrine-Induced Shift in Levels of Adenosine 3’:5’-monophosphate and ATP Parallel to Increased Respiratory Rate and Lipolysis in Isolated Hamster Brown-Fat Cells. *Eur J Biochem* 62: 383–390, 1976. doi: 10.1111/j.1432-1033.1976.tb10170.x.

41. **Rezende EL**, **Hammond KA**, **Chappell MA**. Cold acclimation in peromyscus: Individual variation and sex effects in maximum and daily metabolism, organ mass and body composition. *J Exp Biol* 212: 2795–2802, 2009. doi: 10.1242/jeb.032789.

42. **Dawson N**. The surface-area/body-weight relationship in mice. *Aust J Biol Sci* 20: 687–690, 1967.

43. **Cheung MC**, **Spalding PB**, **Gutierrez JC**, **Balkan W**, **Namias N**, **Koniaris LG**, **Zimmers TA**. Body Surface Area Prediction in Normal, Hypermuscular, and Obese Mice. *J Surg Res* 153: 326–331, 2009. doi:

10.1016/j.jss.2008.05.002.

44. **Gonzalez NC**, **Sokari A**, **Clancy RL**. Maximum oxygen uptake and arterial blood oxygenation during hypoxic exercise in rats. *J Appl Physiol* 71: 1041–1049, 1991. doi: 10.1152/jappl.1991.71.3.1041.

45. **Chacaroun S**, **Vega-Escamilla y Gonzalez I**, **Flore P**, **Doutreleau S**, **Verges S**. Physiological responses to hypoxic constant-load and high-intensity interval exercise sessions in healthy subjects. *Eur J Appl Physiol* 119: 123–134, 2019. doi: 10.1007/s00421-018-4006-9.

46. **Gaikwad AS**, **Ramasarma T**, **Ramakrishna Kurup CK**. Brown adipose tissue mitochondria are cytochrome c - subsaturated. *Mol Cell Biochem* 105: 119–125, 1991. doi: 10.1007/BF00227751.

47. **King L**, **Nielsen S**, **Agre P**. Aquaporin in complex tissues. I. Developmental patterns in respiratory and glandular tissues of rat. *Am J Physiol - Cell Physiol* 273: C1541–C1548, 1997.

48. **Raina S**, **Preston GM**, **Guggino WB**, **Agre P**. Molecular cloning and characterization of an aquaporin cDNA from salivary, lacrimal, and respiratory tissues. *J. Biol. Chem.* 270: 1908–1912, 1995.

49. **Swenson ER**, **Deem S**, **Kerr ME**, **Bidani A**. Inhibition of aquaporin-mediated CO2 diffusion and voltage-gated H+ channels by zinc does not alter rabbit lung CO2 and NO excretion. *Clin Sci* 103: 567–575, 2002. doi: 10.1042/cs1030567.

50. **Foster DO**. Quantitative contribution of brown adipose tissue thermogenesis to overall metabolism. *Can J Biochem Cell Biol* 62: 618–622, 1984.

51. **Shabalina IG**, **Petrovic N**, **deJong JMA**, **Kalinovich A V.**, **Cannon B**, **Nedergaard J**. UCP1 in Brite/Beige adipose tissue mitochondria is functionally thermogenic. *Cell Rep* 5: 1196–1203, 2013. doi: 10.1016/j.celrep.2013.10.044.

52. **Madeira A**, **Mõsca AF**, **Moura TF**, **Soveral G**. Aquaporin-5 is expressed in adipocytes with implications in adipose differentiation. *IUBMB Life* 67: 54–60, 2015. doi: 10.1002/iub.1345.

53. **Chechi K**, **Van Marken Lichtenbelt W**, **Richard D**. Brown and beige adipose tissues: Phenotype and metabolic potential in mice and men. *J Appl Physiol* 124: 482–496, 2018. doi: 10.1152/japplphysiol.00021.2017.

54. **Blondin DP**, **Labbé SM**, **Noll C**, **Kunach M**, **Phoenix S**, **Guérin B**, **Turcotte**

ÉE, **Haman F**, **Richard D**, **Carpentier AC**. Selective impairment of glucose but not fatty acid or oxidative metabolism in brown adipose tissue of subjects with type 2 diabetes. *Diabetes* 64: 2388–2397, 2015. doi: 10.2337/db14-1651.

55. **Liu X**, **Bandyopadhyay B**, **Nakamoto T**, **Singh B**, **Liedtke W**, **Melvin JE**, **Ambudkar I**. A role for AQP5 in activation of TRPV4 by hypotonicity: Concerted involvement of AQP5 and TRPV4 in regulation of cell volume recovery. *J Biol Chem* 281: 15485–15495, 2006. doi: 10.1074/jbc.M600549200.

56. **Yun X**, **Philip NM**, **Jiang H**, **Smith Z**, **Huetsch JC**, **Damarla M**, **Suresh K**, **Shimoda LA**. Upregulation of Aquaporin 1 Mediates Increased Migration and Proliferation in Pulmonary Vascular Cells From the Rat SU5416/Hypoxia Model of Pulmonary Hypertension. *Front Physiol* 12, 2021. doi: 10.3389/fphys.2021.763444.

Tables

	Arterial O_2 Saturation (%) ± SD	**Heart Rate** (min^{-1}) ± SD	n
WT Normoxia	97.9 ± 0.75	573 ± 100	6
KO Normoxia	98.4 ± 0.97	541 ± 69	11
WT Hypoxia	71.7 ± 4.1	493 ± 72	6
KO Hypoxia	71.7 ± 3.1	463 ± 16	10

Table 1. Arterial O_2 saturation and heart rate in WT and AQP5-KO mice under cold exposure in Helox.

	Body weight at start (g)	Body weight after 2 wks 16°C (g)	Body weight after subsequent 2 wks 4°C (g)	Weight of iBAT (mg)	Weight of iBAT per body weight (mg/g)
AQP5-KO					
Mean	24.7	24.4	24.6	**120**	**4.88**
± SD (n)	± 1.9 (6)	± 1.9 (6)	± 1.8 (6)	± 11 (6)	± 0.31 (6)
WT					
Mean	25.7	25.1	25.1	**157**	**6.28**
± SD (n)	± 2.7 (6)	± 2.3 (6)	± 2.0 (6)	± 12 (6)	± 0.62 (6)
P	0.467	0.533	0.64	< 0.0002	< 0.0006

Table 2. Body weights and interscapular BAT weights of AQP5-KO and WT mice after a 4 weeks' graded cold stimulus. All animals were female, average age 300 days. SD, standard deviation, n, number of animals, p, level of significance in a comparison of AQP5-KO vs. WT by unpaired two-sided t-tests.

968

969 ## Figures

970

971

972

973

974

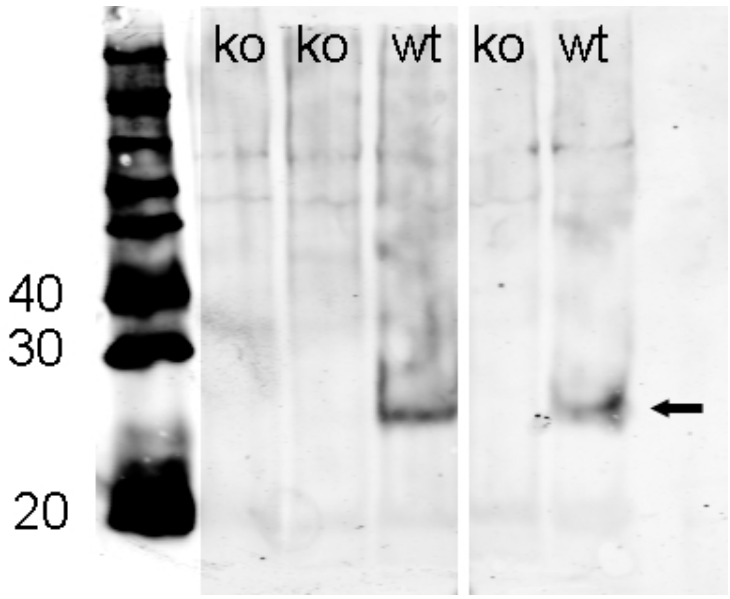

975

976

977 **Fig. 1.** Western Blot of mouse lung tissue homogenate using an antibody against
978 murine AQP5. Arrow indicates AQP5 band at about 27 kDa. On the leftmost lane
979 molecular weight ladder given in kDa (Magic Mark XP, Invitrogen). Ko indicates
980 tissue from AQP5 KO mice, wt tissue from wildtype mice. All lanes are from one
981 blot.

982

983

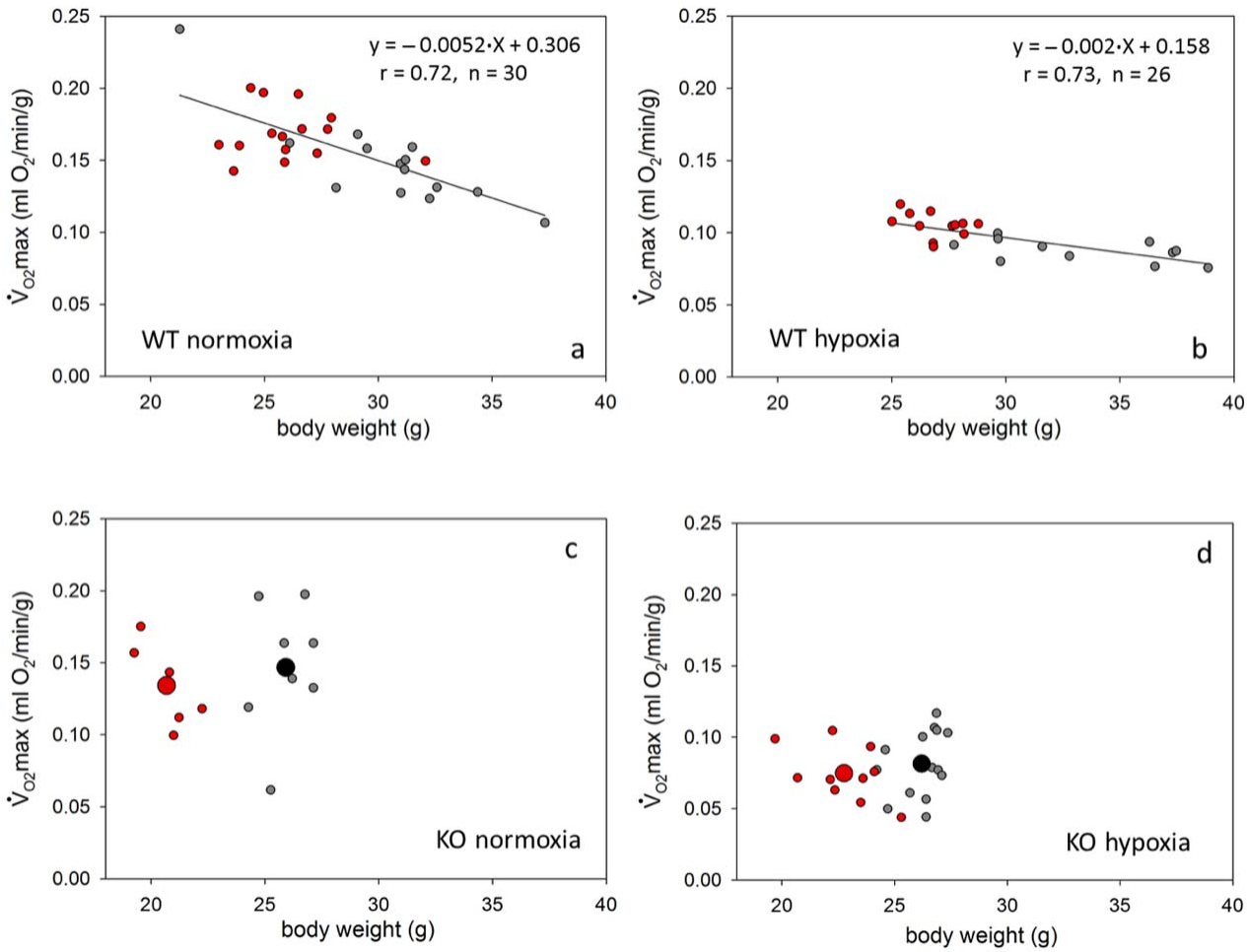

Fig. 2. Specific maximal oxygen consumptions in dependence on body weight. Figs. 2a and 2c, $\dot{V}_{O2,max}$ under normoxia with $pO_{2,insp}$ = 150 mmHg, Figs. 2b and 2d, $\dot{V}_{O2,max}$ under hypoxia with $pO_{2,insp}$ = 80 mmHg. Red dots females, grey dots males. For the WT in Figs. 2a and 2b linear regression lines were calculated as given. For the KO in Figs. 1c and 1d, which are limited to narrower ranges of body weights, averages of the single values are indicated by the big dots.

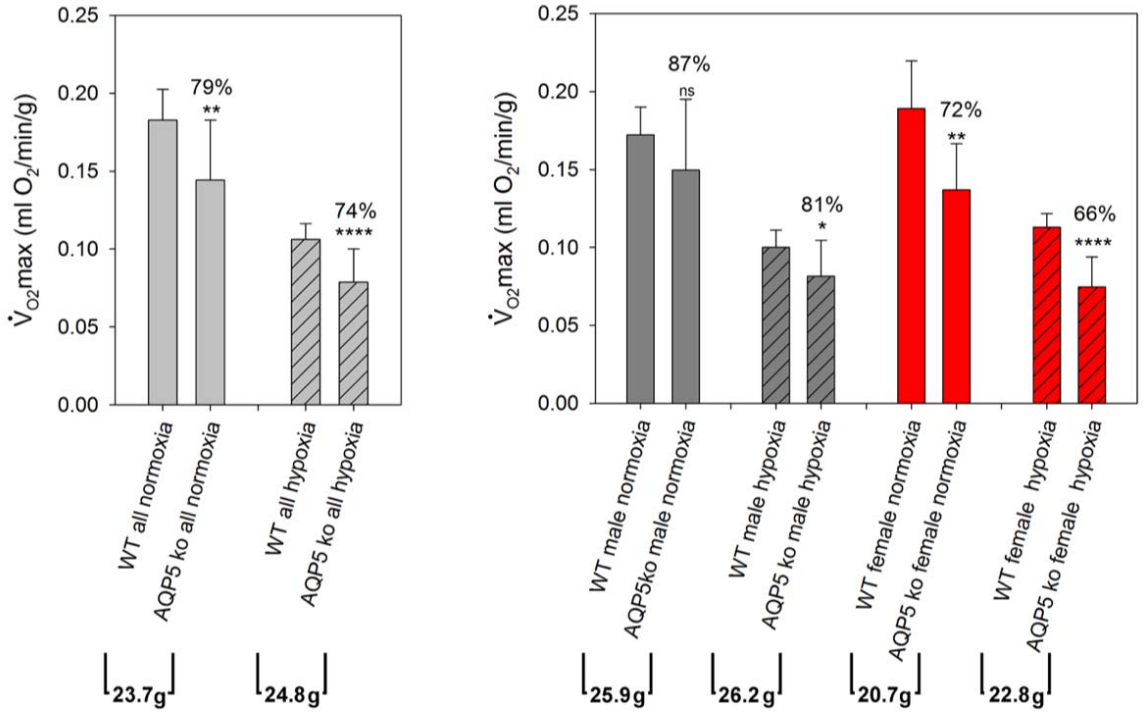

Fig. 3. Average $\dot{V}_{O2,max}$ values for female and male mice combined (left hand side) and for males and females separately (right hand side). Percentages above the columns for KO animals give the percentage of the KO value compared to the corresponding WT value. Error bars indicate SD. Stars indicate the levels of significance of the differences between the data pairs, as determined by t-tests: * P< 0.05, ** P< 0.01, *** P<0.001, **** P< 0.0001. All pairs of columns refer to identical body weights. These weights are those of the KO groups considered. The WT data of $\dot{V}_{O2,max}$ were those shown in Figs. 2a and b, after being corrected to the respective average body weight of the appropriate KO group by using the slopes of the regression lines in Figs. 2a and b. N values of the columns from left to right: 30, 15, 27, 24, 15, 8, 12, 14, 17, 6, 15, 10.

1014

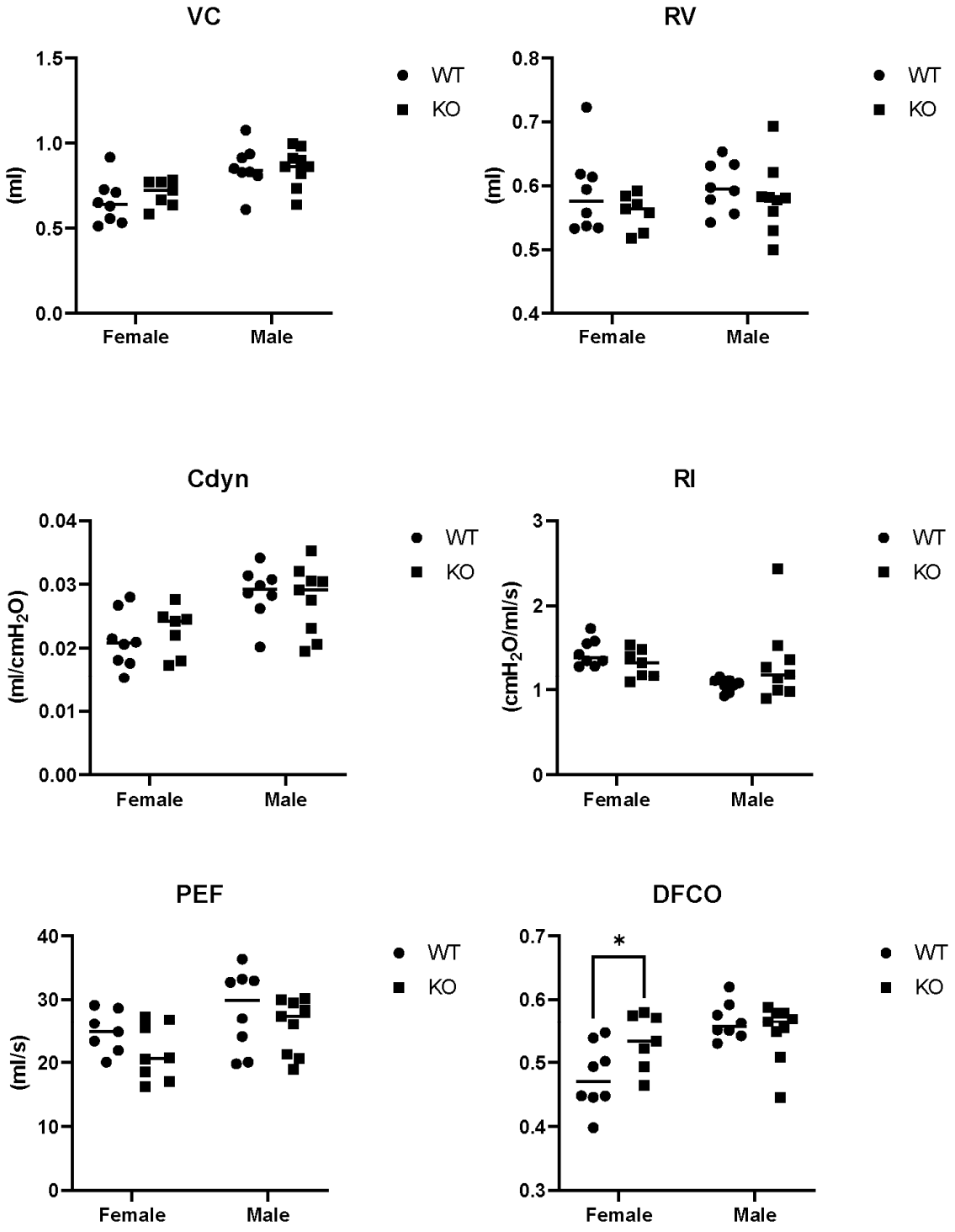

1015

1016

Fig. 4. Functional parameters of the lungs of WT and AQP5-KO mice. VC, vital capacity; RV, residual volume; Cdyn, dynamic compliance; RI, inspiratory resistance; PEF, peak expiratory flow, and DF_{CO}, pulmonary diffusion factor for CO. Statistical analysis was performed by a two-way ANOVA with Sidak's multiple comparison test (GraphPad Prism version 6.01). None of the pairwise comparisons of KO vs. WT showed a statistically significant difference, with the exception of DF_{CO}, which was weakly significant for females ($p=0.035$) but not significant for males ($p=0.67$). Number of animals studied was 8. Additionally, we performed a two-way ANOVA test with interaction with the categories gender and genotype using SPSS (IBM SPSS Statistics, Version 21). This analysis showed globally (i.e. for both sexes combined) no significant difference between KO and WT animals for all different lung parameters (p values between 0.104 and 0.89). Between females and males, significant differences were observed for the parameters VC, Cdyn, PEF and DF_{CO}. No significant interactions between the effects of sex and genotype on parameters were demonstrable for all parameters (p between 0.112 and 0.64), with the exception of DF_{CO} ($p = 0.024$). This latter finding is in accordance with the result seen in the last panel of Fig. 4.